

Topological Insulators in the Frontier of Futuristic Materials

1.1 Introduction:

The primary focus of condensed matter physics revolves around discovering novel phases of matter that drive continuous advancements in electronic devices. According to the band theory of solids, materials are traditionally categorized as metals, semiconductors, or insulators based on their bandgap. A simplified band diagram (Figure 1.1) illustrates the conduction and valence bands, representing higher and lower energy states. The energy gap's size between these bands dictates the material's behavior as a conductor, semiconductor, or insulator.

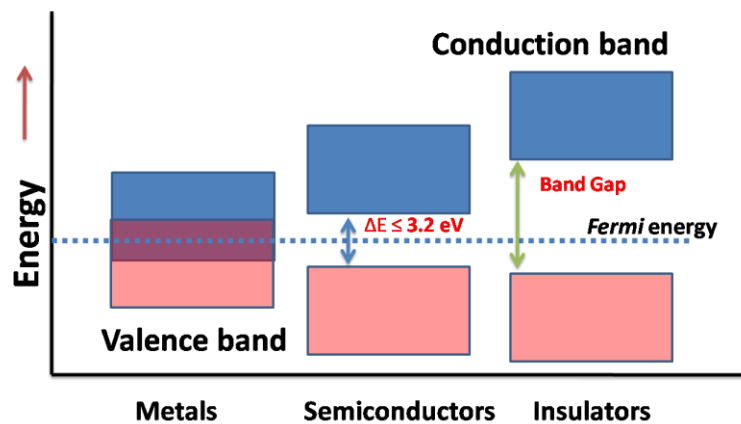


Figure 1.1: Band diagram for metal, semiconductor and insulator

In conductors, the conduction and valence bands overlap, allowing valence electrons unrestricted movement and participation in conduction. On the other hand, insulators possess a wide bandgap ($> 5\text{eV}$), preventing electron conduction due to the significant separation between the conduction and valence bands. Semiconductors exhibit intermediate properties between conductors and insulators.

The discovery of the Quantum Hall Effect unveiled a unique quantum state featuring a conducting surface and an insulating bulk, known as a Topological Insulator (TI). Topological Insulators have captured substantial scientific interest due to their potential for fundamental physics phenomena and technological applications like quantum computing and spintronics. Three-dimensional TIs harbor gapless conducting surface states (SS) that are topologically protected by Time Reversal Symmetry (TRS). The interplay of electron spin and orbital angular momentum results in band inversion phenomena within TIs.

Spin-orbit coupling (SOC) locks the spin-momentum perpendicularly, safeguarding surface states against backscattering by nonmagnetic impurities and defects. This imparts robust electrical conduction at the surface and edge, fostering intriguing properties. TIs offer a platform for Majorana fermions, holding promise for quantum computing, while magnetic TIs may induce magnetic monopoles, showcasing quantum phenomena.

Additional captivating attributes include exciton condensation, quantum anomalous Hall effect (QAHE), topological Hall effect (THE), and topological superconductivity, all relevant for quantum computing and spintronics. The linear energy-momentum relationship of the topological surface state (TSS) within TIs underpins phenomena like Aharonov-Bohm oscillations, weak antilocalization (WAL), and quantum conductance fluctuations.

These phenomena, closely linked with the topological surface state and SOC-driven band inversion near the Fermi level (E_f), lead to captivating magnetotransport properties. Introducing magnetic or nonmagnetic impurities through doping can unveil a range of effects. For instance, magnetically doped TIs can break Time Reversal Symmetry at the Dirac point, allowing tunability of the Fermi level, which significantly influences surface transport properties.

Both two-dimensional and three-dimensional topological insulators have been proposed theoretically and subsequently realized experimentally. To comprehend topological insulators fully, grasping the concept of topology is indispensable

1.2 Topology:

Topology constitutes a mathematical exploration of qualities that endure unchanged during the smooth alteration, twisting, and stretching of objects, all while disallowing tearing and joining. These enduring attributes are referred to as topological properties. Consider two geometric configurations that can be gradually deformed into one another; such equivalence is termed topological equivalence. An illustrative instance involves a coffee mug morphing into a doughnut via smooth deformation, as depicted in Figure 1.2.



Figure 1.2: Schematic representation of topology showing smooth deformation from cup to doughnut.

Nonetheless, certain objects, like an apple, cannot be contorted into a doughnut through such means. In the realm of mathematics, the Gauss-Bonnet theorem establishes a link between the surface's curvature (geometry) and its topology, further associating it with the object's genus. The relationship is expressed as:

$$\frac{1}{2\pi} \oint K \cdot dA = \chi \tag{1.1}$$

Here, the parameter χ is quantized and interconnected with the genus denoted by "g," related via the equation $\chi = 2-2g$. This genus "g" is connected to the count of openings within an object. Objects with identical opening counts are topologically identical. For instance, a coffee mug and a doughnut both possess $g = 1$, while a sphere holds $g = 0$. Hence, a doughnut and a sphere stand as topologically distinct. Consequently, objects sharing the same genus value can be seamlessly transformed into each other, carrying matching topological attributes.

$$\frac{1}{2\pi} \oint_{\text{closed surface}} K dA = 2 - 2g$$


$g = 0$

Gauss-Bonnet theorem
K is Gaussian curvature
g is genus of surface



$g = 1$

Figure 1.3: The sphere and the doughnut are topologically non-equivalent and have different genus numbers.

As depicted in Figure 1.3, the sphere and doughnut stand as topologically disparate entities, distinguished by their varying genus values.

Through the lens of topology theory, the categorization of matter phases, particularly the characterization of insulators, becomes attainable. An insulator's classification hinges on the bandgap that separates its conduction and valence bands. Two insulators can be deemed topologically equivalent if they can transition into one another through adiabatic modifications to their Hamiltonian.

The pivotal element in specifying a matter's state concerning topological classification is embodied in the concept of the Berry phase.

1.3 Berry Phase and Chern number

Berry Phase and Chern Number Within solid-state materials, the Berry phase plays a pivotal role in comprehending diverse phenomena. In the context of crystalline solids, the wave vector K takes on periodic behavior within the Brillouin zone (BZ). This geometric phase finds its association with the Bloch wave function denoted as $|u_m(K)\rangle$, where K signifies momentum within the BZ. This Berry phase is defined based on the fluctuations of the Bloch function across the BZ. Generally, the Berry phase can be mathematically captured through a line integral as follows:

$$A_m(K) = i \langle u_m | \Delta_k | u_m \rangle \quad (1.2)$$

Where A_m is a vector (in terms of Bloch wavefunction). The surface integral of Berry curvature is;

$$F_m(K) = \Delta_k \times A_m(K) \quad (1.3)$$

The total Berry Flux in BZ may be expressed;

$$n = \frac{1}{2\pi} \int_{\text{BZ}} d^2k F_m(K) \quad (1.4)$$

In this equation, the variable "n" assumes the role of an integer, commonly referred to as the Chern number. This Chern number stands as a topological invariant, assuming significance when the Hamiltonian undergoes smooth variations. According to the findings of Hasan and Kane, when the Chern number "n" equals 0, the insulator is categorized as trivial. Conversely, when "n" equals 1, it corresponds to a quantum spin Hall insulator [1]. In more detail, a trivial insulator manifests a gapped edge state, while a nontrivial insulator presents an edge state characterized by a gapless helical structure—a distinctive feature setting it apart from the trivial insulator."

1.4 Time-Reversal Symmetry (TRS)

Time-Reversal Symmetry (TRS) The concept of order, a fundamental principle in condensed matter physics, offers insight into the understanding of Topological Insulators (TIs). In this field, phases of matter, such as solids and liquids, are often deciphered through the lens of symmetry. The Landau theory of phase transitions elucidates that these shifts occur due to the breaking of symmetries. For instance, during the transition from liquid to solid, translational symmetry is disrupted, while rotational symmetry is shattered in the phase change of a liquid. Complex phases like ferromagnetism (with broken rotational symmetry) and superconductivity (arising from broken gauge symmetry) emerge through symmetry breaking.

However, the elegance of the topological insulator lies in the preservation of a specific symmetry, namely time-reversal symmetry (TRS). Time-reversal symmetry plays a pivotal role in safeguarding the topological surface state (TSS) of TIs. This protective effect stems from the fact that the edge states in two dimensions (2D) and surface states in three dimensions (3D) of TIs remain robust against the presence of nonmagnetic impurities or defects. Consequently, these states exhibit an absence of backscattering.

This intriguing behavior is a consequence of the phenomenon known as spin-momentum locking. In the presence of strong spin-orbit coupling (SOC), electrons exhibit a distinctive trait: they can solely move in the forward direction. The robustness of the TSS lies in the fact that no spin configuration is available for a backward trajectory without reversing the spin's direction. This linkage between the electron's spin and its momentum is linear, enforcing a unidirectional movement. This inherent property enhances the appeal of TIs, as it paves the way for the development of dissipationless devices and a host of other applications.

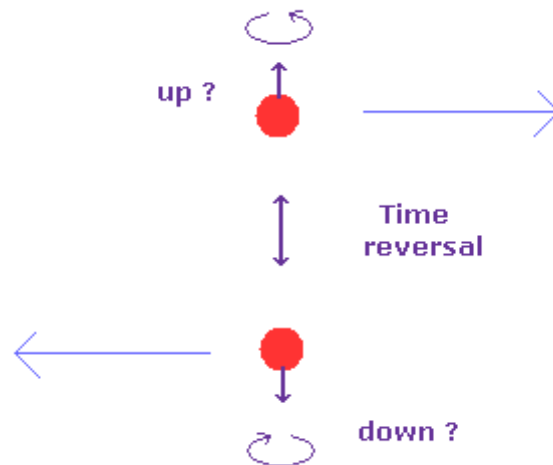


Figure 1.4: Schematic diagram of motion of two electrons having opposite spins with preservation of TRS in TSS.

Visualized in Figure 1.4, the schematic diagram illustrates the coordinated motion of two electrons with opposing spins, underscoring the preservation of time-reversal symmetry within the topological surface state (TSS).

1.5 Background of Topological Insulator

1.5.1 Hall Effect:

The foundation of the topological insulator concept has roots in the discovery of the Hall effect, pioneered by Edwin Hall in 1879 [10]. When a conducting slab or metal is subjected to both an electric field and a perpendicular magnetic field, the charge carriers experience both the Lorentz force and the electric field's influence. This leads to the accumulation of equal and opposite charges on opposite faces of the material, resulting in the generation of a voltage across the conductor. This phenomenon is known as the Hall effect, illustrated in Figure 1.5. Utilizing the Hall effect, it becomes possible to deduce the carrier concentration and determine the nature of the charge carriers.

Consider, for example, an n-type semiconductor as depicted in Figure 1.5. In this scenario, the charge carriers are electrons (e^-). These electrons move with a velocity (v) perpendicular to the applied magnetic field, generating the Lorentz force (eVB), where e represents the electron charge and B signifies the magnetic field in the z -direction. Consequently, a negative charge accumulation occurs on the downward face of the conductor, giving rise to a potential difference between the top and bottom surfaces of the slab.

By applying an electric field (E_H), an upward force (eE_H) is exerted on the electrons to maintain equilibrium, leading to the following expressions:

$$eE_H = eVB \quad (1.5)$$

$$E_H = VB \quad (1.6)$$

The current density (J_x) in the direction of x can be written as;

$$J_x = neV \quad (1.7)$$

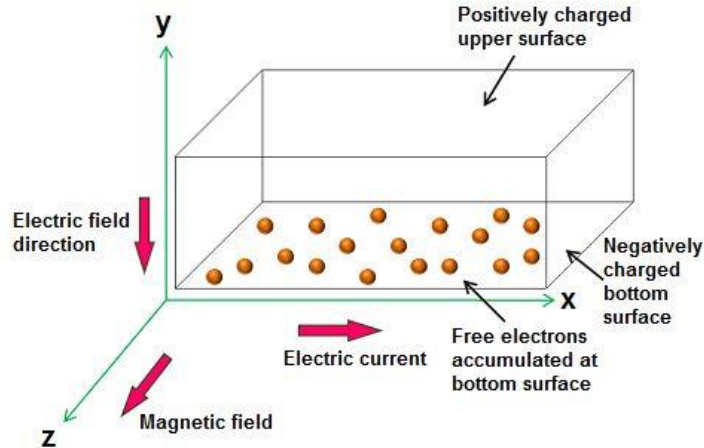


Figure 1.5: Schematic diagram of Hall effect (<https://www.physics-and-radio-electronics.com/electronic-devices-and-circuits/semiconductor/halleffect.html>)

Where n is the carrier concentration, hence;

$$E_H = \frac{BJ_x}{ne} \quad (1.8)$$

The Hall coefficient can be defined as;

$$E_H = R_H BJ_x \quad (1.9)$$

$$R_H = \frac{E_H}{BJ_x}; \quad (1.10)$$

$$R_H = \frac{1}{n_e} \quad (1.11)$$

In the case of n-type semiconductor;

$$R_H = -\frac{1}{n_e} \quad (1.12)$$

The negative sign signifies that the electric field develops in the negative y-direction, indicating that the charge carriers are electrons.

1.5.2 Effect of the magnetic field in 3D system

Upon the application of a strong magnetic field in a three-dimensional system, a range of captivating phenomena emerges, including the quantization of energy levels, exemplified through Landau Levels, as well as distinct oscillatory behaviors within electrical resistivity (SdH Oscillations) and magnetization (de

Haas-van Alphen Effect), among others. These intricate properties arise due to the energy's quantized nature.

When a magnetic field is directed along the z-axis (B_z), electrons (e^-) do not experience any force in the direction of the applied magnetic field. Consequently, the movement of electrons in the z-direction remains unaltered. Drawing parallels to the principles of the quantum harmonic oscillator, electrons function as if they are unimpeded in the z-direction while being quantized in the x and y-directions. This characteristic energy of electrons can be expressed as:

$$E_n = \left(n + \frac{1}{2} \right) \hbar \omega_c + \frac{\hbar^2 K_z^2}{m_e^*}, \text{ where } n = 0, 1, 2, 3, \dots \quad (1.13)$$

Here, 'n' denotes the Landau level number, 'me' stands for the effective mass of electrons, 'Kz' represents the momentum vector of electrons in the z-direction, and ω_c symbolizes the cyclotron frequency. The frequency ω_c can be comprehended as:

$$\omega_c = \frac{eB_z}{m_e^*} \quad (1.14)$$

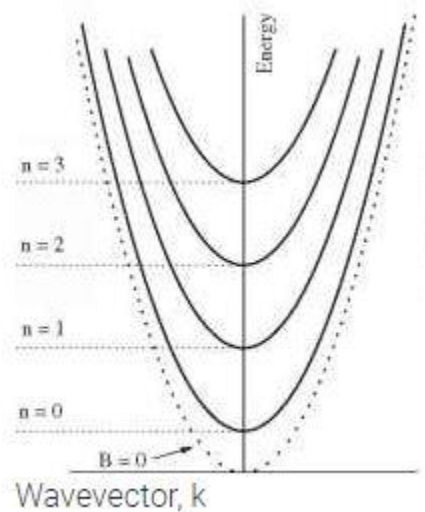


Figure 1.6: Energy band diagram for electrons vs wave vector for different Landau levels in 3D system [https://www.texaspowerfulsmart.com/quantum-wells/chapter-7-1.html]

Visualized in Figure 1.6, the energy band diagram portrays the relationship between electrons' energy and wave vector, showcasing diverse Landau levels within a three-dimensional system [https://www.texaspowerfulsmart.com/quantum-wells/chapter-7-1.html].

1.5.3 Effect of the magnetic field in 2D system

When a two-dimensional (2D) system is exposed to the XY plane and a magnetic field is introduced along the z-direction, the electrons (e^-) encounter a force within the XY plane. As a consequence, the energy

levels undergo quantization, following a model akin to the quantum harmonic oscillator. In this configuration, the energy of the system is expressed as:

$$E_n = (n + \frac{1}{2}) \hbar \omega_c, \text{ where } n=0,1,2,3,\dots \quad (1.15)$$

In this equation, 'n' signifies the Landau level number, 'm^{*}' represents the effective mass of electrons, 'k_z' denotes the momentum vector of electrons in a specific direction, and ω_c stands for the cyclotron frequency. The frequency ω_c can be comprehended as:

$$\omega_c = \frac{eB_z}{m_e^*} \quad (1.16)$$

1.5.4 Quantum Hall Effects (QHE)

The inception of the topological insulator concept is closely linked to the discovery of the Quantum Hall Effect (QHE). In 1980, Von Klitzing made the groundbreaking observation of QHE in a two-dimensional (2D) system subjected to a strong magnetic field at low temperatures, subsequently being awarded the Nobel Prize in 1985 [1], [11]. Unlike the classical Hall effect, the Hall conductance exhibited complete quantization.

This quantization is expressed by the equation:

$$\sigma_{xy} = n \frac{e^2}{h} \quad (1.17)$$

Here, 'n' represents an integer, 'h' denotes the Planck constant, and 'e' signifies the charge of an electron. The phenomenon finds its explanation in the quantization of electron motion within the cyclotron orbit. Consequently, energy levels are also quantized into discrete Landau levels, expressed as:

$$E_n = (n + \frac{1}{2}) \hbar \omega_c \quad (1.18)$$

Furthermore, the cyclotron frequency can be understood through:

$$\text{And} \quad \omega_c = \frac{eB}{m} \quad (1.19)$$

Where 'n' is an integer, 'B' stands for the perpendicular magnetic field, and 'm' represents the electronic cyclotron mass. The Fermi energy resides between two adjacent Landau levels, leading to insulating behavior. Hall conductivity displays complete quantization, as outlined in equation (1.17), illustrated as plateau-like behavior in Figure 1.7.

Key features of the Quantum Hall Effect include:

1. A high magnetic field is necessary.
2. Time-Reversal Symmetry (TRS) is not preserved.
3. Quantum hall conductance values are highly precise.

4. Longitudinal resistivity (equivalent conductivity) becomes negligible.

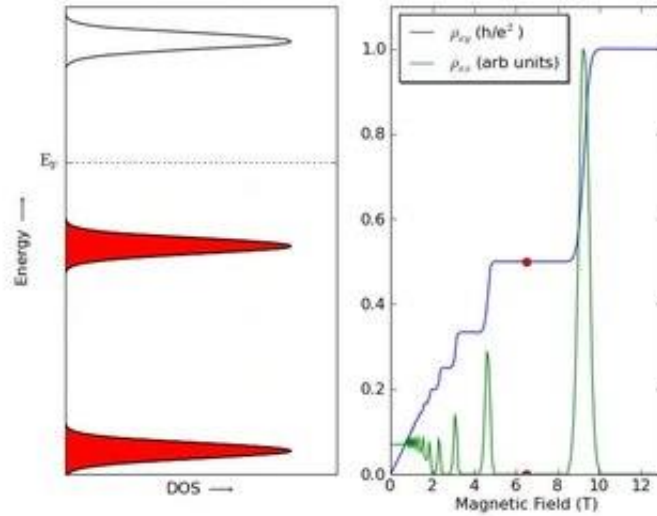


Figure 1.7: Quantization of energy levels into discrete Landau levels under the applied magnetic field (left) and the variation in longitudinal (ρ_{xx}) and transverse resistivity (ρ_{xy}) with applied magnetic field showing QHE. (https://en.wikipedia.org/wiki/Quantum_Hall_effect)

As illustrated in Figure 1.7, electrons follow quantized circular cyclotron orbits, fostering insulating behavior. At the material's edge, electrons are permitted to move along skipping orbits, leading to a unidirectional charge flow depending on the magnetic field direction. These states, known as 'edge states,' pertain to the skipping orbits.

The unidirectional charge propagation engenders chiral behavior at the upper and lower edges. Within the edge state, backscattering does not occur due to the inability of charge carriers to reverse their direction of motion.

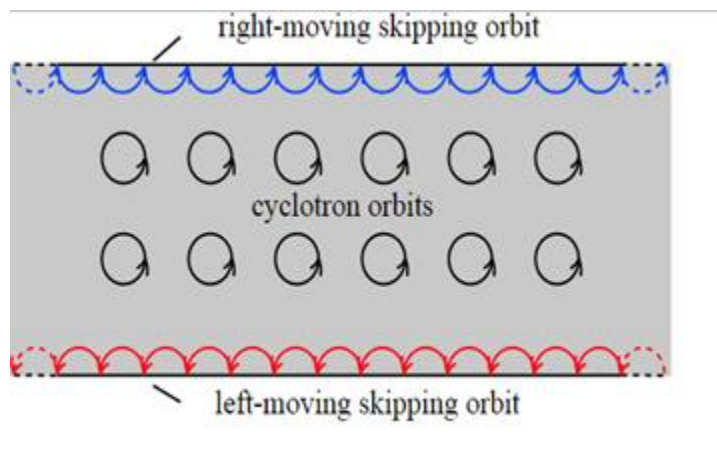


Figure 1.8: Depicts the skipping orbits at the edge state and the cyclotron orbits in the bulk of a 2D electron gas in the presence of a magnetic field.

1.5.5 Quantum Spin Hall Effect (QSHE)

The Quantum Spin Hall Effect (QSHE) serves as a fundamental element within the realm of 2D topological insulators. This phenomenon was propelled by the discovery of the Quantum Hall Effect (QHE), which spurred theoretical explorations into systems capable of mimicking the conductive behavior exhibited in QHE but without the need for an external magnetic field. Unlike QHE, the QSHE operates without the reliance on an external magnetic field, as the intrinsic Spin-Orbit Coupling (SOC) generates the requisite magnetic field. In 2005, Kane and Mele proposed a model that essentially combines two copies of QHE, each with an opposing spin and magnetic field, culminating in the emergence of the QSHE [12].

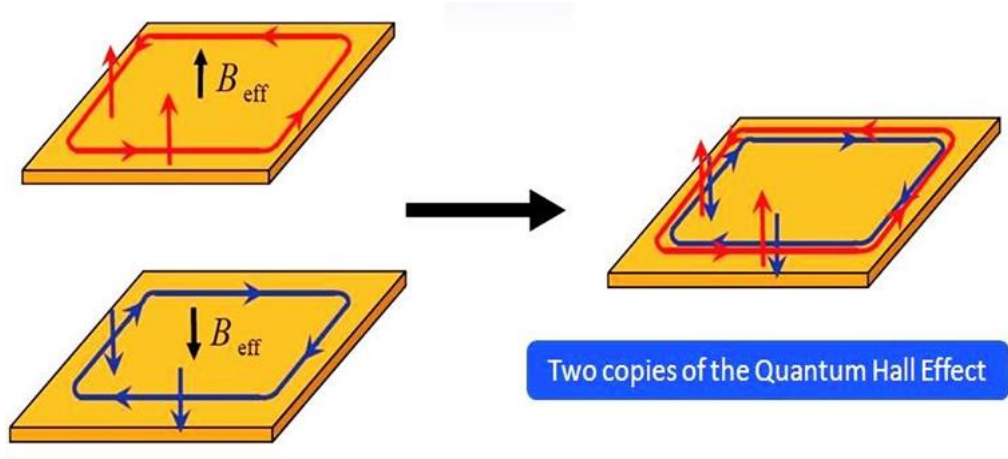


Figure 1.9: Two copies of the quantum Hall effect (QHE) with the opposite magnetic field (left) and (right) the amalgamation of these two QHE states makes a quantum spin Hall effect (QSHE) without applied magnetic field (Adapted from [12]).

This QSHE scenario is illustrated in Figure 1.9, where two instances of the Quantum Hall effect (QHE) are juxtaposed with opposite magnetic fields, leading to the amalgamation of these QHE states to create the Quantum Spin Hall Effect (QSHE) without any applied magnetic field.

Within QSHE, both upper and lower sections of the sample harbor right-moving and left-moving electrons, with spin orientations oriented up and down, respectively. These spin-polarized edge states remain resilient against scattering due to non-magnetic impurities. Rather than undergoing backscattering, electrons navigate around the impurity, ensuring that backscattering is suppressed in the QSHE, as depicted in Figure 1.10.

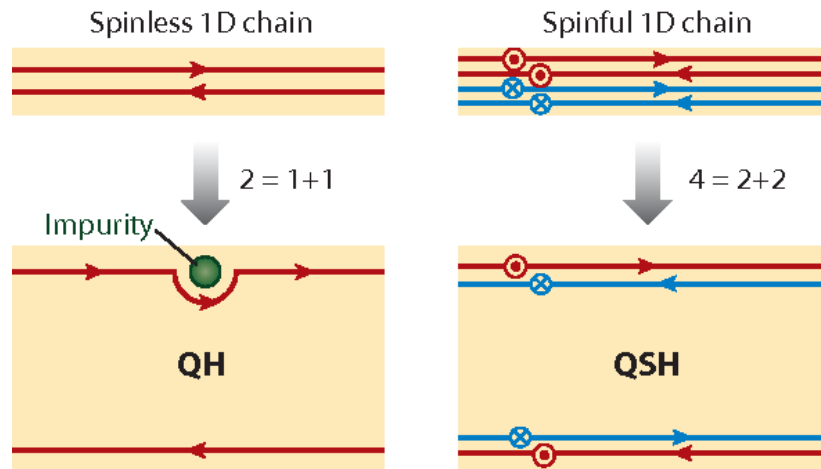


Figure 1.10: (Left) QHE with both right moving and left moving edge states. These states are robust against backscattering. (Right) QSHE with upper state right moving spin up and left moving spin down. Backscattering is suppressed from nonmagnetic impurities (adapted from [13])

The suppression of backscattering can be understood through the behavior of electrons encountering an impurity. As showcased in Figure 1.11, when a spin-up electron encounters an impurity, it can backscatter via two distinct paths: clockwise and anticlockwise rotations around the impurity. These paths introduce phase differences of π and $-\pi$, respectively, culminating in a net 2π phase difference. Consequently, these two wave functions undergo destructive interference, facilitating dissipationless transport [13].

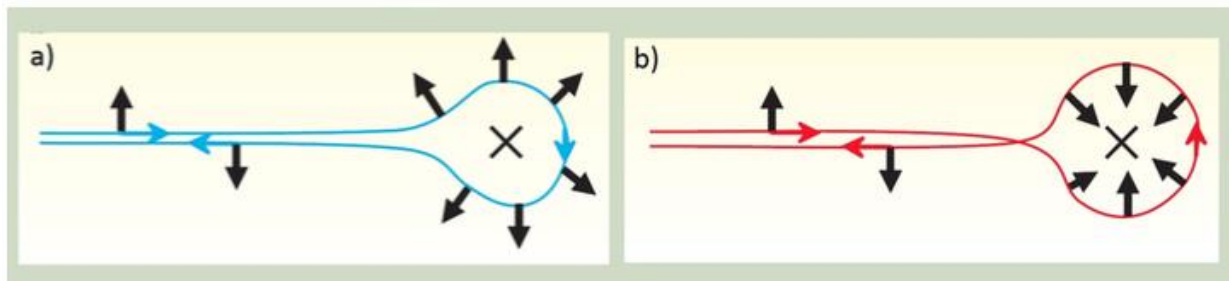


Figure 1.11: schematic diagram of two opposite scattering paths around an impurity for the QSH state. The total path difference between them is 2π , leading to suppression of the backscattering for Fermions (adapted from [13]).

However, the introduction of a magnetic impurity or the application of a magnetic field in a topological insulator erases the preservation of Time-Reversal Symmetry (TRS).

The quest for QSHE initially looked to graphene; however, its weak SOC hindered this endeavor. The presence of heavy elements with robust SOC is crucial for the manifestation of 2D TIs, as SOC is a relativistic term. In 2006, Bernevig et al. [15] theoretically predicted that the QSHE might manifest in a HgTe quantum

well. This structure involves a thin layer of HgTe, rich in SOC, sandwiched between two layers of CdTe to create a 2D quantum well structure. Following this prediction, Konig et al. experimentally confirmed the quantized conductance of $2e^2/h$ at zero magnetic fields in HgTe in 2007, thereby establishing HgTe quantum well as the first known 2D Topological Insulator [16].

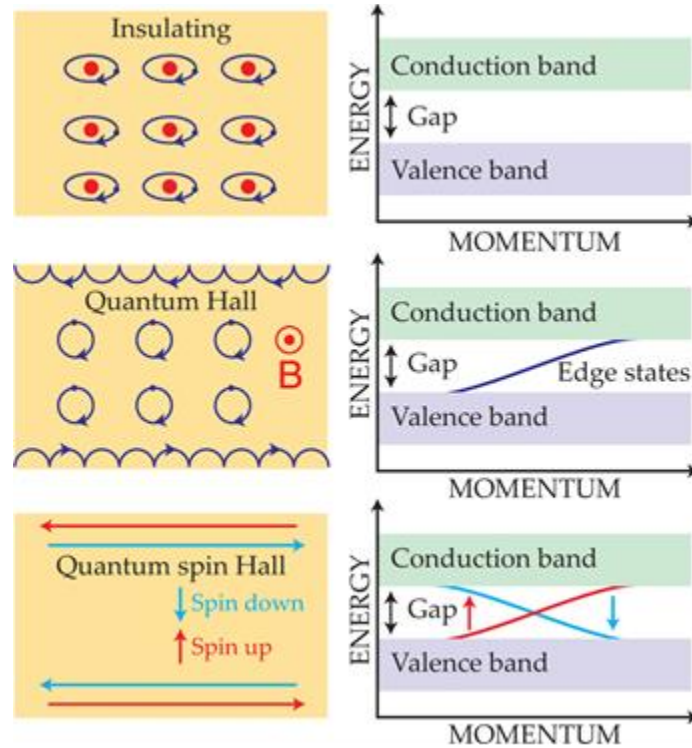


Figure 1.12: Depicts (a) an insulating state characterized by a bandgap between conduction and valence bands [14], (b) the bulk's insulating nature coexisting with electron conduction at the edges through skipping orbits, resulting in conduction edges and no band gap [14], (c) the QSHE scenario where both left and right moving paths of electrons with opposing spins are permissible, all safeguarded by Time-Reversal Symmetry [14].

1.5.6 Spin-orbit coupling

When the intrinsic angular momentum or spin of an electron interacts with its orbital angular momentum, the phenomenon known as Spin-Orbit Coupling (SOC) emerges. In conventional materials, such as semiconductors, the conduction band is formed by electrons in s orbitals, while the valence band consists of electrons in p orbitals. This leads to the upward shift of the conduction band (s-band) and the downward shift of the valence band (p-band) [13]. As a result, in ordinary materials, these bands do not intersect. However, in materials where the SOC is substantial, the valence band (p-band) shifts upward, and the conduction band (s-band) shifts downward. This shift in bands causes their crossing, leading to a

phenomenon called band inversion [5], [17]. This inversion, driven by strong SOC, results in the valence band's energy becoming higher than that of the conduction band.

At the point where these bands intersect, conducting states emerge, giving rise to the surface state. In this scenario, the bandgap vanishes at the surface state, rendering it a metallic surface state.

Within the Topological Surface State (TSS), spin-up and spin-down electrons encounter alternating effective magnetic fields, compelling them to propagate in opposite directions. This interplay is referred to as spin-momentum locking, offering valuable applications. The spin state corresponds to the applied current direction at the surface. Reversing the applied current direction causes a corresponding reversal in the spin state, a property that holds promise for data storage and switching device applications.

A particularly intriguing facet of spin-momentum locking in Topological Insulators is its role in preventing backscattering of electron motion. For instance, considering a spin-up electron propagating forward, its spin is intrinsically tied to its momentum. Backscattering would necessitate the transformation of the spin-up electron into a spin-down electron, an implausible scenario due to the absence of an available opposite spin state. This protection from backscattering is upheld by both spin-momentum locking and the preservation of Time-Reversal Symmetry (TRS), unless TRS is disrupted (as in the presence of a magnetic impurity). Consequently, these combined mechanisms fortify the resilience of the TSS against backscattering.

It's important to note that the aforementioned explanation applies to an odd number of forward or backward-moving channels. For systems with an even number of channels, backscattering can indeed occur.

1.5.7 Quantum Anomalous Hall Effect (QAHE)

In nonmagnetic materials, the Hall voltage exhibits proportionality to the applied magnetic field due to the influence of the Lorentz force, as we have previously discussed in detail. The curve's slope manifests a linear field dependence and is dictated by the characteristics and charge density of the carriers. Following the discovery of the conventional Hall effect (OHE), Hall conducted analogous experiments on ferromagnetic materials and noted a remarkable and substantial slope, particularly at low magnetic fields. Subsequent investigations revealed that this peculiar behavior stemmed from the spontaneous magnetization intrinsic to ferromagnetic materials. This supplementary phenomenon, occurring in conjunction with the ordinary Hall effect, came to be known as the anomalous Hall effect (AHE), as depicted in Figure 1.13.

Given that ferromagnetic materials can exhibit spontaneous magnetization even in the absence of a magnetic field, the anomalous Hall effect (AHE) can be observed without the presence of an external

magnetic field. While it is widely believed that spin-orbit coupling (SOC) plays a pivotal role in producing the anomalous Hall effect (AHE), the exact mechanism remains somewhat elusive. Other factors, such as skew scattering or the side jump of carriers (extrinsic mechanisms), as well as intrinsic mechanisms, might also contribute to the AHE [18]. The quantum mechanical manifestation of the anomalous Hall effect is termed the quantum anomalous Hall effect (QAHE).

Following the identification of the quantum anomalous Hall effect, researchers swiftly recognized that the theories utilized to elucidate the Quantum Hall Effect (QHE) could potentially be applied to explain the occurrence of QAHE in magnetic materials.

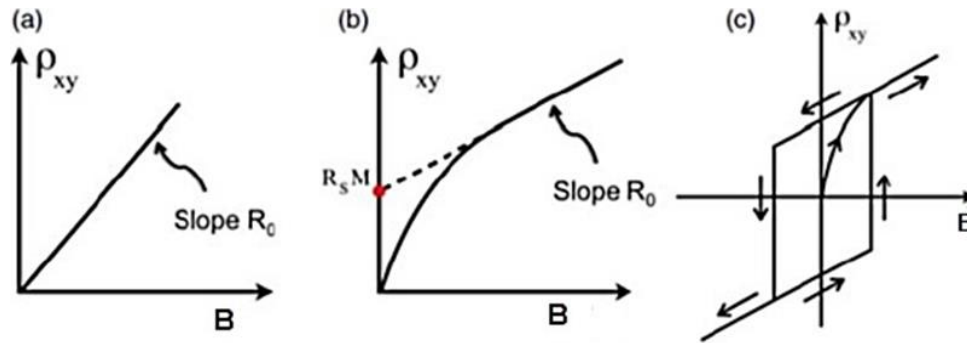


Figure 1.13: Depicts the alterations in Hall resistivity ρ_{xy} concerning the applied magnetic field B , including (a) the ordinary Hall effect (b) the anomalous Hall effect (AHE), and (c) the measured hysteresis loop stemming from the quantum anomalous Hall effect (QAHE) [18].

1.5.8 Shubnikov-de Haas (SdH) Oscillations

When a 2D electron gas is subjected to a powerful magnetic field at low temperatures, its energy levels become divided into discrete energy states known as Landau levels, as previously explained in section (1.5.3). The substantial magnetic field forces electrons into localized motion, tracing out cyclotron orbits with a frequency of $\omega_c = eB/m^*$, where e signifies the electron's charge, B stands for the magnetic field strength, and m^* denotes the effective electron mass. The energy of each Landau level, E_n , adheres to the equation (1.18):

$$E_n = \left(n + \frac{1}{2} \right) \hbar \omega_c$$

As the magnetic field strength escalates, the gap between successive Landau levels widens. Consequently, with increasing magnetic field strength, the position of Landau levels shifts. This shift transpires rapidly, causing the Fermi level to temporarily coincide with certain Landau levels. During this interval, electrons leap between occupied levels (below the Fermi energy) and unoccupied levels (above the Fermi energy). In this process, electrons encounter scattering within these Landau levels, leading to a discernible peak in

the graph depicting resistivity against magnetic field strength. Conversely, when the Fermi level resides between two Landau levels, scattering diminishes, resulting in the absence of a peak within the resistivity versus magnetic field graph. This oscillatory pattern observed in resistivity is termed Shubnikov-de Haas (SdH) oscillation. If similar oscillations manifest in the magnetization versus magnetic field graph, they are referred to as de Haas-van Alphen (dHvA) oscillations.

1.6 Historical Developments of 2D and 3D Topological Insulators

1.6.1 First 2D topological insulator HgTe

Shubnikov-de Haas oscillations exclusively arise under a perpendicular magnetic field in a 2D electron gas, while in a 3D electron gas, SdH oscillations can be observed in various directions. Notably, SdH oscillations offer insights into the Berry phase [19]. These oscillations facilitate the determination of crucial parameters such as effective mass, surface carrier density, dingle temperature, quantum mobility, and the mapping of the Fermi surface.

The prediction of the Quantum Spin Hall (QSH) state's existence centered around a HgTe quantum well that is enveloped between two thin layers of CdTe. In 2006, Bernevig presented this unique HgTe heterostructure, where the thickness of the HgTe layer (dHgTe) is flanked by two equally thick layers of CdTe (dCdTe) [1], [13], [14]. The HgTe heterostructure's electronic band structure, particularly at the Γ point, showcases an intriguing inverted arrangement. This peculiar configuration is significantly influenced by the thickness of the HgTe layer, as it governs the confinement energy and subsequently shifts the energy bands. As the HgTe layer thickness, denoted as 'd,' approaches a critical value, $d = d_c$, the Quantum Spin Hall Effect (QSHE) materializes without the need for an external magnetic field. The CdTe/HgTe/CdTe heterostructure, along with the band structures of HgTe and CdTe, is illustrated in Figure 1.15. The corresponding band structures for varying widths of the quantum well 'd' are depicted in the same figure. Crucially, after surpassing the critical width d_c , a band inversion occurs at the Γ point. This leads to the emergence of 1-D helical edge states, and a 2-D quantum well's boundaries become the sites of band inversion.

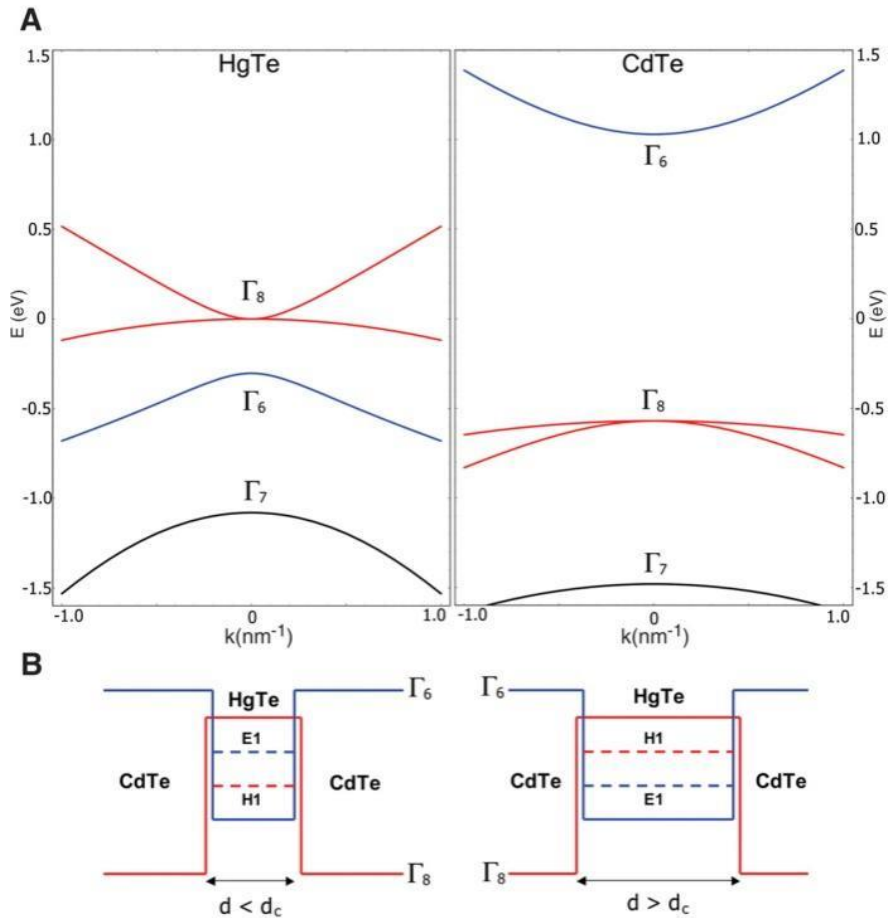


Figure 1.15: (a) bulk energy bands for HgTe and CdTe at Γ point (b) CdTe/HgTe/CdTe quantum well in normal regime $d < d_c$ and in inverted regime $d > d_c$ (Adapted from [13]).

Upon reaching the critical thickness d_c , set at 6.3 nm, the energy bandgap completely diminishes, resulting in the touching of the Dirac cones at a particular point called the Dirac point. Subsequent experimental investigations have substantiated the presence of the Quantum Spin Hall Effect in HgTe quantum well systems. This empirical support is further bolstered by experimental evidence demonstrating the spin polarization of the QSH edge state.

1.6.2 3D Topological Insulators

After the initial development of 2D topological insulators, the concept of 3D topological insulators emerged through the contributions of Moore and Balents [22], Roy [23], and Fu, Kane, and Mele[24]. While 2D topological systems feature conducting edges, their 3D counterparts exhibit conducting surface states. In the realm of 3D topological insulators, the band structure of these surface states can be

described as a 2D state characterized by the dispersion of a singular Dirac cone. Notably, strong topological insulators are distinguished by an odd number of Dirac cones.

Within the context of 3D topological insulators, four Z_2 topological invariants ($\nu_0, \nu_1, \nu_2, \nu_3$) come into play, with ν_0 pertaining to the strong topological invariant, and $\nu_1 - \nu_3$ corresponding to the weak topological invariant. A ν_0 value of 1 in strong topological insulators signifies the presence of an odd number of Dirac cones on the surface. Of particular interest is the phenomenon of spin-momentum locking perpendicular to the surface state of 3D topological insulators. In this intriguing manifestation, a state possessing momentum K and $-K$ exhibits opposite spins—up spins propagate in the $+x$ direction, while down spins traverse the $-x$ direction. This distinctive behavior results in the prevention of backscattering within the surface state of the topological insulator, rendering the surface state highly robust.

1.6.3 The First 3D Topological Insulator $\text{Bi}_{1-x}\text{Sb}_x$

Shortly after the experimental validation of the 2D Quantum Spin Hall (QSH) state in HgTe quantum wells, a significant milestone was achieved in 2008 when Hsien et al.[25] reported the first experimental evidence of the 3D Topological Insulator (TI) state in the material $\text{Bi}_{1-x}\text{Sb}_x$. The exploration of charge transport in 3D materials is notably more intricate compared to their 2D counterparts due to the influence of bulk effects. Consequently, establishing topological signatures at the surface state becomes more challenging. To address this complexity, Angle-Resolved Photoemission Spectroscopy (ARPES) emerged as a valuable tool to investigate the surface states that are inherently topologically protected. ARPES involves utilizing photons to eject electrons from a crystal, revealing information about the surface and bulk electronic structures through the examination of the ejected electron's momentum. This technique enables the differentiation of bulk band structures from surface states since surface states do not disperse perpendicular to the surface[1].

A robust topological insulator is characterized by a linear dispersion relation, with the metallic surface state crossing the Fermi level at an odd number of points. The ARPES spectrum of $\text{Bi}_{1-x}\text{Sb}_x$ is depicted in Figure 1.16, revealing that the surface state crosses the Fermi energy five times. Following Kramer's theorem, this odd number of crossings signifies topologically protected states in $\text{Bi}_{0.9}\text{Sb}_{0.1}$. However, capturing the topological surface state in $\text{Bi}_{1-x}\text{Sb}_x$ is inherently intricate in nature[1].

Subsequently, in 2009, Zhang et al.[26] theoretically predicted certain chalcogenide compounds (A_2B_3) as 3D topological insulators through ab initio functional theory. The non-trivial surface states and calculated bulk bandgaps of Bi_2Se_3 , Sb_2Te_3 , and Bi_2Te_3 are illustrated in Figure 1.16. The experimentally verified band

structures in these materials were effectively revealed using ARPES. The ARPES spectrum of Bi_2Se_3 , displayed in Figure 1.16, distinctly exhibits linear dispersion in the surface state, and the presence of a Dirac cone within the band structure confirms its identity as a topological insulator.

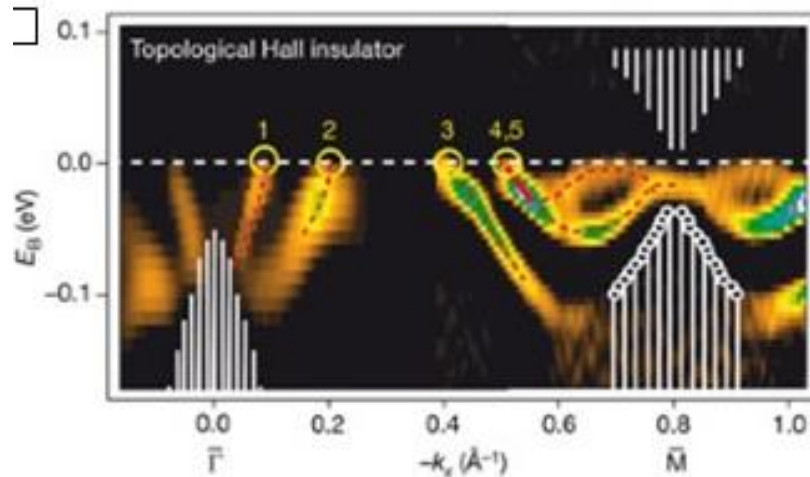


Figure 1.16: The surface band dispersion second-derivative image of $\text{Bi}_{0.9}\text{Sb}_{0.1}$. there are five crossing between Γ and M which confirms topological non-trivial surface state (Adapted from [6]).

1.6.4 New materials Bi_2Se_3 , Bi_2Te_3 and Sb_2Te_3

Bi_2Se_3 stands as the most extensively investigated Topological Insulator (TI) to date; however, it is not without imperfections, rendering the retrieval of the topological surface state in transport experiments a challenging endeavor. Figure 1.17 offers a clear depiction of the non-trivial states in Bi_2Se_3 , Sb_2Te_3 , and Bi_2Te_3 . Notably, the calculated band gap for Bi_2Te_3 measures 100 meV, Sb_2Te_3 demonstrates 260 meV, and

Bi_2Se_3 showcases 300 meV. Much like $\text{Bi}_{1-x}\text{Sb}_x$, these materials - Bi_2Se_3 , Bi_2Te_3 , and Sb_2Te_3 - possess the same strong topological invariant, prompting an extensive body of research dedicated to exploring their properties. Unlike $\text{Bi}_{1-x}\text{Sb}_x$, these materials are inherently pure, avoiding the complexities associated with alloys. Consequently, the preparation of these materials in a high-purity state is feasible [6], [27].

Furthermore, these materials distinctly exhibit the topological surface state in ARPES spectra, coupled

with the advantageous feature of a sizable bandgap even at room temperature.

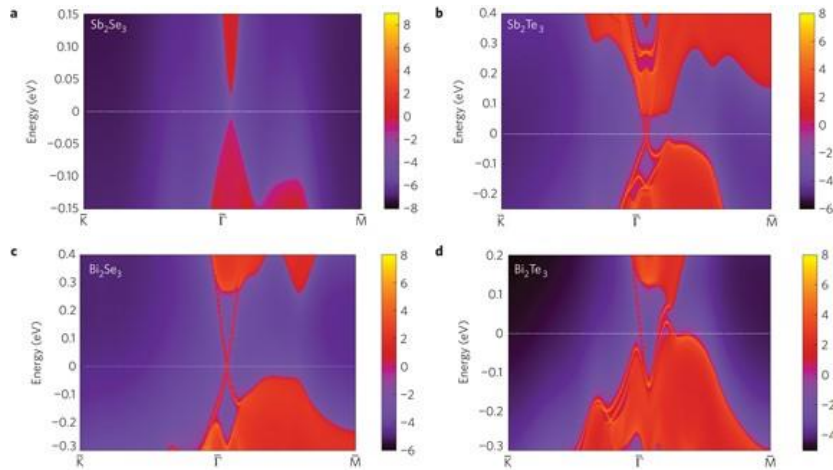


Figure 1.17: Calculated band structure of Sb_2Se_3 , Sb_2Te_3 , Bi_2Se_3 and Bi_2Te_3 by ab initio density functional theory. Red represents occupied bulk and surface states, and blue signifies bulk band gap[6]

The combination of these characteristics positions them as excellent candidates for Topological Insulators. Consequently, these materials represent the most extensively studied systems within the realm of Topological Insulators.

References:

- [1] M. Z. Hasan and C. L. Kane, "Colloquium: Topological insulators," *Rev. Mod. Phys.*, vol. 82, no. 4, pp. 3045–3067, 2010, doi: 10.1103/RevModPhys.82.3045.
- [2] S. Lee, "Dirac Surface States of Magnetic Topological Insulators," pp. 4–13, 2017, [Online]. Available: <https://psu.app.box.com/file/248078760600>.
- [3] J. Teng, N. Liu, and Y. Li, "Mn-doped topological insulators: A review," *J. Semicond.*, vol. 40, no. 8, 2019, doi: 10.1088/1674-4926/40/8/081507.
- [4] J. Kim and S. H. Jhi, "Magnetic phase transition in Fe-doped topological insulator Bi_2Se_3 ," *Phys. Rev. B - Condens. Matter Mater. Phys.*, vol. 92, no. 10, pp. 1–5, 2015, doi: 10.1103/PhysRevB.92.104405.
- [5] Z. Zhu, Y. Cheng, and U. Schwingenschlög, "Band inversion mechanism in topological insulators: A guideline for materials design," *Phys. Rev. B - Condens. Matter Mater. Phys.*, vol. 85, no. 23, pp. 1–5, 2012, doi: 10.1103/PhysRevB.85.235401.

- [6] M. Z. Hasan and J. E. Moore, "Three-Dimensional Topological Insulators," *Annu. Rev. Condens. Matter Phys.*, vol. 2, no. 1, pp. 55–78, 2011, doi: 10.1146/annurev-conmatphys-062910-140432.
- [7] W. Qin and Z. Zhang, "Persistent ferromagnetism and topological phase transition at the interface of a superconductor and a topological insulator," *Phys. Rev. Lett.*, vol. 113, no. 26, pp. 1–5, 2014, doi: 10.1103/PhysRevLett.113.266806.
- [8] H. B. Zhang, H. L. Yu, D. H. Bao, S. W. Li, C. X. Wang, and G. W. Yang, "Weak localization bulk state in a topological insulator Bi₂Te₃ film," *Phys. Rev. B - Condens. Matter Mater. Phys.*, vol. 86, no. 7, pp. 1–7, 2012, doi: 10.1103/PhysRevB.86.075102.
- [9] J. G. Analytis, R. D. McDonald, S. C. Riggs, J. H. Chu, G. S. Boebinger, and I. R. Fisher, "Two-dimensional surface state in the quantum limit of a topological insulator," *Nat. Phys.*, vol. 6, no. 12, pp. 960–964, 2010, doi: 10.1038/nphys1861.
- [10] C. Felser and X. L. Qi, "Topological insulators," *MRS Bull.*, vol. 39, no. 10, pp. 843–846, 2014, doi: 10.1557/mrs.2014.217.
- [11] F. Tang *et al.*, "Three-dimensional quantum Hall effect and metal–insulator transition in ZrTe₅," *Nature*, vol. 569, no. 7757, pp. 537–541, 2019, doi: 10.1038/s41586-019-1180-9.
- [12] H. Buhmann, "The quantum spin hall effect," *J. Appl. Phys.*, vol. 109, no. 10, pp. 1–6, 2011, doi: 10.1063/1.3577612.
- [13] X. L. Qi and S. C. Zhang, "Topological insulators and superconductors," *Rev. Mod. Phys.*, vol. 83, no. 4, 2011, doi: 10.1103/RevModPhys.83.1057.
- [14] L. Muechler, B. Yan, F. Casper, S. Chadov, and C. Felser, "Topological Insulators," *Springer Ser. Mater. Sci.*, vol. 182, no. 02, pp. 123–139, 2013, doi: 10.1007/978-3-642-37537-8_6.
- [15] I. B. Cohen and S. E. Morison, "References and Notes," *Some Early Tools Am. Sci.*, no. December, pp. 177–190, 2014, doi: 10.4159/harvard.9780674368446.c10.
- [16] M. König, L. W. Molenkamp, X. Qi, and S. Zhang, "in HgTe Quantum Wells," *Science (80-.)*, vol. 766, no. 2007, pp. 766–771, 2010.
- [17] H. Li *et al.*, "Negative magnetoresistance in Dirac semimetal Cd₃As₂," *Nat. Commun.*, vol. 7, pp. 1–7, 2016, doi: 10.1038/ncomms10301.
- [18] N. Nagaosa, J. Sinova, S. Onoda, A. H. MacDonald, and N. P. Ong, "Anomalous Hall effect," *Rev. Mod. Phys.*, vol. 82, no. 2, pp. 1539–1592, 2010, doi: 10.1103/RevModPhys.82.1539.
- [19] J. Xiong, Y. Luo, Y. Khoo, S. Jia, R. J. Cava, and N. P. Ong, "High-field Shubnikov-de Haas oscillations in the topological insulator Bi₂Te₂Se," *Phys. Rev. B - Condens. Matter Mater. Phys.*, vol. 86, no. 4, pp. 1–6, 2012, doi: 10.1103/PhysRevB.86.045314.
- [20] J. J. Cha, D. Kong, S. S. Hong, J. G. Analytis, K. Lai, and Y. Cui, "Weak antilocalization in Bi₂(Se_{1-x}Te_x)₃ nanoribbons and nanoplates," *Nano Lett.*, vol. 12, no. 2, pp. 1107–1111, 2012, doi: 10.1021/nl300018j.

- [21] S. X. Zhang *et al.*, “Magneto-resistance up to 60 Tesla in topological insulator Bi₂Te₃ thin films,” *Appl. Phys. Lett.*, vol. 101, no. 20, pp. 2–6, 2012, doi: 10.1063/1.4766739.
- [22] J. E. Moore and L. Balents, “Topological invariants of time-reversal-invariant band structures,” *Phys. Rev. B - Condens. Matter Mater. Phys.*, vol. 75, no. 12, pp. 3–6, 2007, doi: 10.1103/PhysRevB.75.121306.
- [23] R. Roy, “Topological phases and the quantum spin Hall effect in three dimensions,” *Phys. Rev. B - Condens. Matter Mater. Phys.*, vol. 79, no. 19, pp. 1–5, 2009, doi: 10.1103/PhysRevB.79.195322.
- [24] L. Fu, C. L. Kane, and E. J. Mele, “Topological insulators in three dimensions,” *Phys. Rev. Lett.*, vol. 98, no. 10, pp. 1–4, 2007, doi: 10.1103/PhysRevLett.98.106803.
- [25] D. Hsieh *et al.*, “A topological Dirac insulator in a quantum spin Hall phase (experimental realization of a 3D Topological Insulator),” vol. 974, no. November 2007, pp. 970–974, 2009, [Online]. Available: <http://arxiv.org/abs/0910.2420>.
- [26] X. L. Qi, R. Li, J. Zang, and S. C. Zhang, “Inducing a magnetic monopole with topological surface states,” *Science (80-.)*, vol. 323, no. 5918, pp. 1184–1187, 2009, doi: 10.1126/science.1167747.
- [27] Y. L. Chen *et al.*, “Massive dirac fermion on the surface of a magnetically doped topological insulator,” *Science (80-.)*, vol. 329, no. 5992, pp. 659–662, 2010, doi: 10.1126/science.1189924.